U.S. DEPARTMENT OF ENERGY | Office of Science

DOE/SC-CM-23-001

FY2023 First Quarter Performance Metric: Improving Simulations of Atmospheric Rivers and Heat Waves in the Coupled E3SM

Bryce E. Harrop, Pacific Northwest National Laboratory
L. Ruby Leung, Pacific Northwest National Laboratory
Paul A. Ullrich, University of California, Davis

January 2023

DISCLAIMER

Contents

1.0 Product Definition 1
2.0 Product Documentation 1
3.0 Results 2
3.1 Atmospheric Rivers 2
3.2 Heat Waves 7
4.0 References 10

Figures

Figure 1. NDJFM AR frequency for ERA5 (a) and the difference in AR frequency between E3SM-HR and ERA5 (b) and E3SM-LR and ERA5 (c). 3
Figure 2. Regions used to examine the 850 hPa winds associated with landfalling ARs and the histograms of these winds for each region. All values are in units of m/s. 4
Figure 3. Histograms for precipitation associated with landfalling ARs. IMERG precipitation values are used (with ERA5 tracked AR objects) for observations. All values are in units of mm/day. 5
Figure 4. PDFs of ARs with size greater than $1x10^{12}$ m^2. AR length and width are based on Principal Component Analysis of the AR shape, and have units of great circle distance. 6
Figure 5. Zonal winds averaged between over the Northern Pacific (180-110W) for NDJFM for ERA5 (a), and the differences between E3SM-HR and ERA5 (b) as well as E3SM-LR and ERA5 (c). The black contours in each panel are equal to the climatological ERA5 values. Units are given in m/s. 6
Figure 6. MJJAS 95th percentile daily maximum temperature for ERA5 (a). Differences between E3SM-HR and ERA5 (b) and between E3SM-LR and ERA5 (c). Units are K. 7
Figure 7. Heat wave frequency in ERA5, and differences between E3SM-HR and ERA5, as well as E3SM-LR and ERA5. Units are number of days. 8
Figure 8. As in Figure 7, only for HW intensity. Units are K. 9
Figure 9. As in Figure 7, only for HW duration. Units are number of days. 9

1.0 Product Definition

The Western US is subject to many natural hazards, such as floods, droughts, heat waves, and fires. Continued investments in modeling efforts from the Department of Energy (DOE) have enabled examination of some of these hazards with the Energy Exascale Earth System Model (E3SM) at high spatial resolution – 25 km grid spacing compared to the standard, or low resolution, 100 km grid spacing.

Atmospheric Rivers (ARs) are filamentary bands of increased atmospheric moisture transport. Nearly all poleward moisture transport out of the subtropics occurs through ARs (Zhu & Newell, 1998). ARs have been shown to be a valuable source of freshwater supplies, while also having the capacity to bring about flooding, landslides, and wind damage, making them a key component of the hydrologic cycle to understand. Models like E3SM are a critical tool for predicting variabilities and changes in ARs, but uncertainties remain regarding which aspects of modeling, such as horizontal resolution, may improve the representation of ARs.

Heat waves (HWs) are periods of extreme near-surface temperatures that last on the order of days. As the global mean temperature has increased, so too have the frequency and intensity of HWs (Seneviratne, 2021). HWs are especially concerning, owing to their links to increased morbidity (Ye et al., 2012), only to be exacerbated by increasing average temperatures under a warming climate (Huang et al., 2011). Like ARs, models have biases in representing these events.

The DOE-sponsored TempestExtremes software product (Ullrich & Zarzycki, 2017; Ullrich et al., 2021) allows for tracking of ARs and HWs as objects. TempestExtremes has been used to track ARs repeatedly in the past (e.g., Liu et al., 2022; Rhoades et al., 2021). HWs, to date, have primarily been examined using timeseries analysis performed at individual locations. Here, we leverage TempestExtremes recently developed object-tracking capability within a new methodological framework to examine HWs as widespread events instead of using a traditional point-wise evaluation.

In this document, we evaluate the performance of E3SM in simulating ARs impacting the US West Coast and HWs in the Western US. As part of the Phase 1 water cycle simulation campaign, E3SMv1 was used to perform simulations at high resolution (~25 km grid spacing) and low resolution (~100 km grid spacing) to evaluate the impacts of model resolution on representing water cycle processes. Both ARs and HWs are thus examined at high and low resolutions and the differences are compared and summarized herein. Results show the impact of increased resolution on ARs is mixed, with some features showing improvements (capturing wind and precipitation extremes) while others showing degradation (frequency, position, and shape). Increased resolution improves HW intensity and duration, while HW frequency is rather insensitive to the model resolutions examined.

2.0 Product Documentation

This report analyzes fully-coupled simulations from the E3SMv1 high-resolution (E3SM-HR) and low-resolution (E3SM-LR) experiments, as detailed in Caldwell et al. (2019) following a similar protocol of the Coupled Model Intercomparison Project Phase 6 (CMIP6) HighResMIP experiments (Haarsma et al. 2016). Both E3SM-HR and E3SM-LR have active atmosphere, land, ocean, sea-ice, and river components. The atmosphere model is described by Rasch et al. (2019) and makes use of a 72-level

spectral element dynamical core to solve the primitive equations (Dennis et al., 2012). Parameterized processes include deep convection (Neale et al., 2008; Richter & Rasch, 2008; Zhang & McFarlane, 1995); macrophysics, turbulence, and shallow convection (Golaz et al., 2002; Larson, 2017; Larson & Golaz, 2005); microphysics (Gettelman & Morrison, 2015; Gettelman et al., 2015); aerosol treatment (Liu et al., 2016; Wang et al., 2020); and radiative transfer (Iacono et al., 2008; Mlawer et al., 1997). The ocean and sea-ice models use the Model for Prediction Across Scales (Petersen et al., 2019; Ringler et al., 2013), and a mesoscale eddy parameterization (Gent & Mcwilliams, 1990) is used for E3SM-LR only. The land model is based on the Community Land Model version 4.5 (Oleson et al., 2013), run with satellite phenology. The river model is the Model for Scale Adaptive River Transport (Li et al., 2013; Li et al., 2015), using runoff simulated by the land model to compute channel velocity, channel water depth, and water surface area and simulate streamflow.

E3SM-HR and E3SM-LR use an identical set of physical parameters but differ in the horizontal grid-spacing of each model component. Each component has approximately a factor of four grid refinement. The atmosphere and land components share a grid with spacing roughly equal to 25 km for E3SM-HR and 110 km for E3SM-LR. The ocean and sea-ice models also share a grid. The ocean/sea-ice grid varies in resolution globally, spanning 8-16 km for E3SM-HR and 30-60 km for E3SM-LR.

To track ARs and HWs, we use the TempestExtremes software (Ullrich & Zarzycki, 2017). ARs are tracked as features with large (area exceeding 850000 km2), localized vertically-integrated water vapor transport, that do not also fit the criteria for Tropical Cyclones (warm core low pressure systems). HWs are tracked as features whose daily maximum temperature exceeds the 95th percentile temperature for that location and during the May through September period for at least two consecutive days. In both cases, metrics like AR and HW frequency are sensitive to the specific feature definition chosen (e.g., Shields et al., 2018), which has implications for evaluating model performance in simulating these extreme events (Leung et al., 2022). Investigating the impacts of such sensitivity on our model evaluation results is beyond the scope of this study but should be explored in the future.

After tracking of ARs and HWs in the E3SM HR and LR simulations and in observations, different aspects of these extreme events are analyzed and compared between the HR and LR simulations and the observations.

3.0 Results

3.1 Atmospheric Rivers

We begin with an analysis of the simulated ARs at high- and low-resolution in E3SMv1. We use the ERA5 reanalysis (Hersbach et al., 2020) as a baseline to assess whether any differences between HR and LR are improvements to the simulation. While ERA5 may have its own biases, in general it tends to perform well when compared to other reanalyses across numerous metrics (Hersbach et al., 2020 and citations therein). Because ERA5 relies on parameterizations for producing precipitation, we combine ERA5 tracked ARs with precipitation from the IMERG product (Huffman et al., 2017) as a benchmark for AR precipitation distributions.

We begin by examining the November through March (NDJFM) frequency of ARs in ERA5 and the difference between both model simulations and ERA5. Improvement is quantified using both the well-

known root mean square error (RMSE) and index of agreement (IoA). The IoA complements the RMSE in quantitatively assessing the performance of E3SM with respect to ERA5, and is computed as

$$1-\frac{\sum_{i=1}^{N}\left(o_i-p_i\right)^2}{\sum_{i=1}^{N}\left(\left|p_i-\overline{o}\right|+\left|o_i-\overline{o}\right|\right)^2}$$

where o_i is the observation (ERA5), p_i is the model prediction, and $\overline{o}$ is the mean of the observations. The value of IoA ranges between 0 and 1, with values closer to 1 indicating better agreement. Unlike RMSE which measures the magnitude of model errors and the Pearson correlation coefficient which measures the linear relationship between the simulated and observed values, IoA can detect both additive and proportional differences in the observed and simulated means and variances.

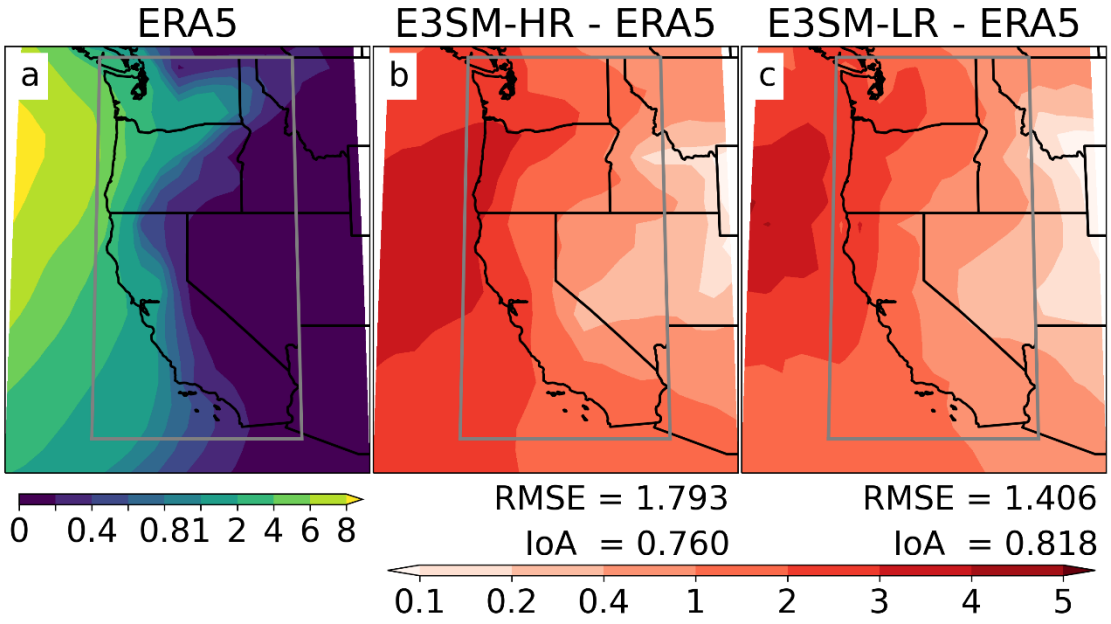

Figure 1. NDJFM AR frequency for ERA5 (a) and the difference in AR frequency between E3SM-HR and ERA5 (b) and E3SM-LR and ERA5 (c).

Both versions of E3SM produce an over-abundance of ARs relative to ERA5. The bias structure is quite similar for both E3SM-HR and E3SM-LR, but there is an increase in bias magnitude for E3SM-HR relative to E3SM-LR. The similarity in AR frequency bias suggests that the number of landfalling ARs is not very sensitive to resolution in E3SM.

Next, we examine the 850 hPa winds associated with landfalling ARs (Figure 2), as ARs are marked by both anomalous moisture and strong winds that combine to transport significant moisture across the

subtropics. All three datasets have been remapped to a uniform 1x1 degree grid to make for a fair comparison.

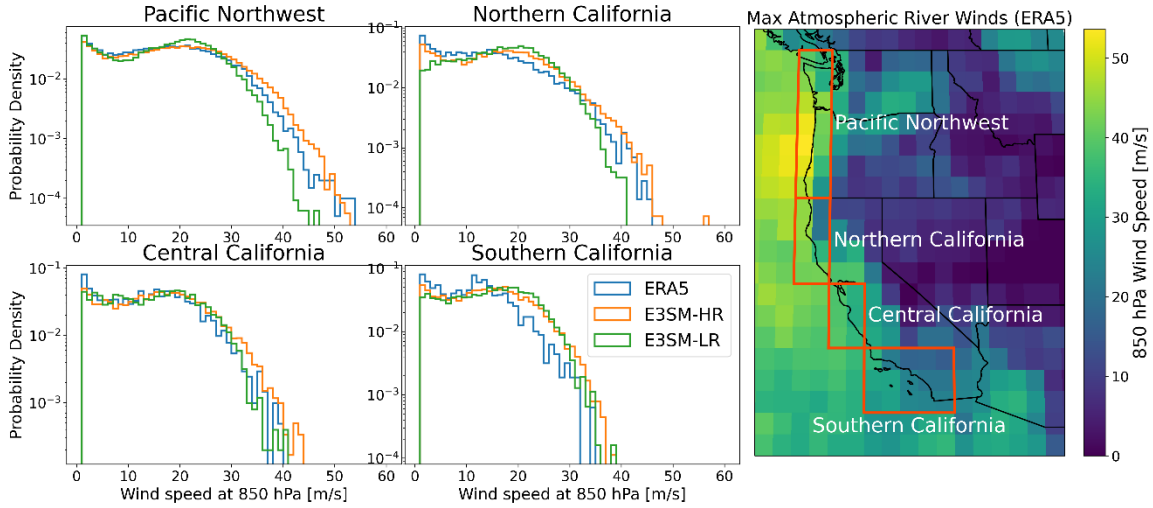

Figure 2. Regions used to examine the 850 hPa winds associated with landfalling ARs and the histograms of these winds for each region. All values are in units of m/s.

The US West Coast is sub-divided into four regions: the Pacific Northwest, Northern California, Central California, and Southern California (Figure 2). Significant improvements to the structure of the PDF of winds can be seen for the Pacific Northwest and Northern California with the increase in horizontal resolution. For these two regions, E3SM-LR is incapable of producing the extreme wind events associated with ARs that occur in ERA5. However, E3SM-HR does significantly better at capturing these wind storms. For Central and Southern California, the differences are less obvious, with both E3SM-LR and E3SM-HR capturing the general structure of the ERA5 PDF.

In addition to winds associated with landfalling ARs, it is useful to examine precipitation from ARs because of its role in driving flooding. Figure 3 shows the precipitation distribution for landfalling ARs over the same regions shown in Figure 2. E3SM-HR produces more intense rainfall events, an expected consequence of its better representation of topographic variations and sharp gradients in the integrated vapor transport. For the Pacific Northwest and Northern California, both E3SM-HR and E3SM-LR underestimate the intensity of extreme precipitation associated with ARs, though E3SM-HR shows significant improvements over E3SM-LR. For Central California, E3SM-HR matches IMERG reasonably well, but over Southern California, E3SM-HR overestimates the tail of AR rainfall. Overall, between the winds and precipitation, AR extremes are better captured by E3SM-HR than E3SM-LR, making it a more suitable tool than E3SM-LR for understanding and predicting these extremes.

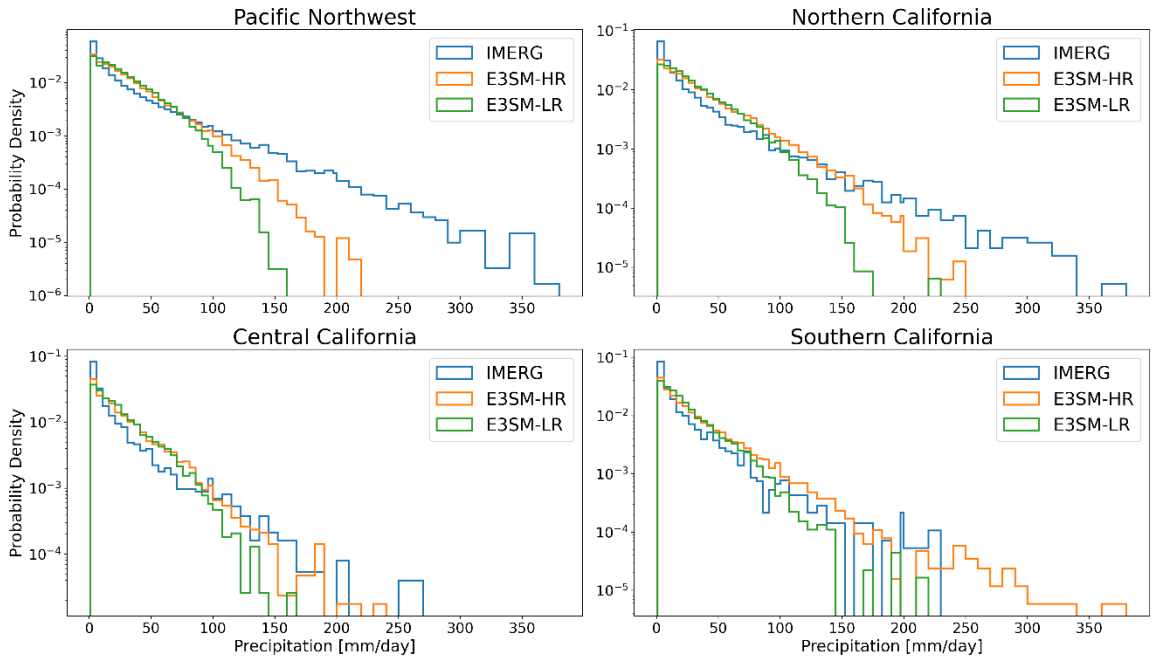

Figure 3. Histograms for precipitation associated with landfalling ARs. IMERG precipitation values are used (with ERA5 tracked AR objects) for observations. All values are in units of mm/day.

Next, we examine the geometry of ARs. We use Principal Component Analysis (PCA) following Inda-Díaz et al. (2021) to quantify the centroid longitude and latitude, as well as the length and width of ARs. Figure 4 shows the PDFs of these quantities for E3SM-LR, E3SM-HR, and ERA5. E3SM-LR outperforms E3SM-HR for all four quantities when compared to ERA5. Both E3SM-HR and E3SM-LR produce too many poleward ARs, but E3SM-HR also produces too many equatorward ARs. The overabundance of equatorward ARs is likely a result of a stronger equatorward jet bias in E3SM-HR than E3SM-LR (Figure 5). An equatorward jet bias, a common feature of global climate models, has been linked to AR frequency bias (Hagos et al., 2016), consistent with the larger AR frequency bias in HR than LR seen in Figure 1. Closer to the surface, Figure 5 shows biases both equatorward and poleward of the mean ERA5 jet position for E3SM-HR, consistent with the poleward and equatorward centroid latitude biases of E3SM-HR shown in Figure 4. The length scales associated with stirring and mixing of the mid-latitude circulation increase farther poleward (Lu et al., 2015; Lu et al., 2018), suggesting the length and width biases in E3SM-HR are connected to the mean wind biases in E3SM-HR. It is beyond the scope of this report to identify an exact cause for the bias in the mean circulation and how it varies with model resolution.

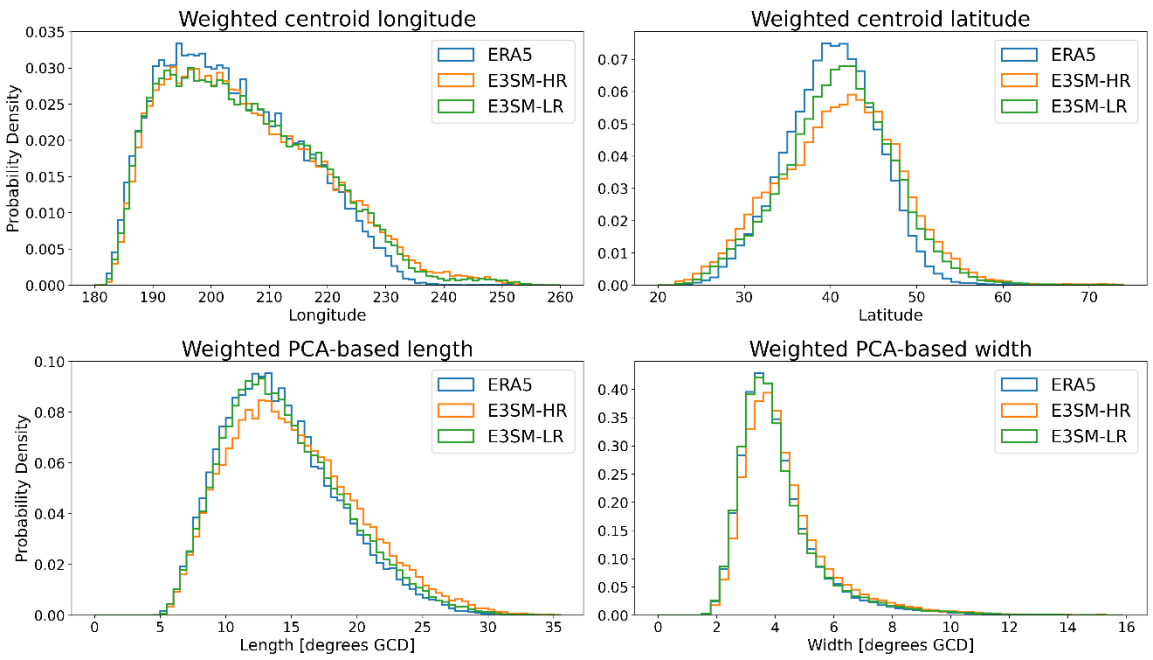

Figure 4. PDFs of ARs with size greater than $1x10^{12}$ m^2. AR length and width are based on Principal Component Analysis of the AR shape, and have units of great circle distance.

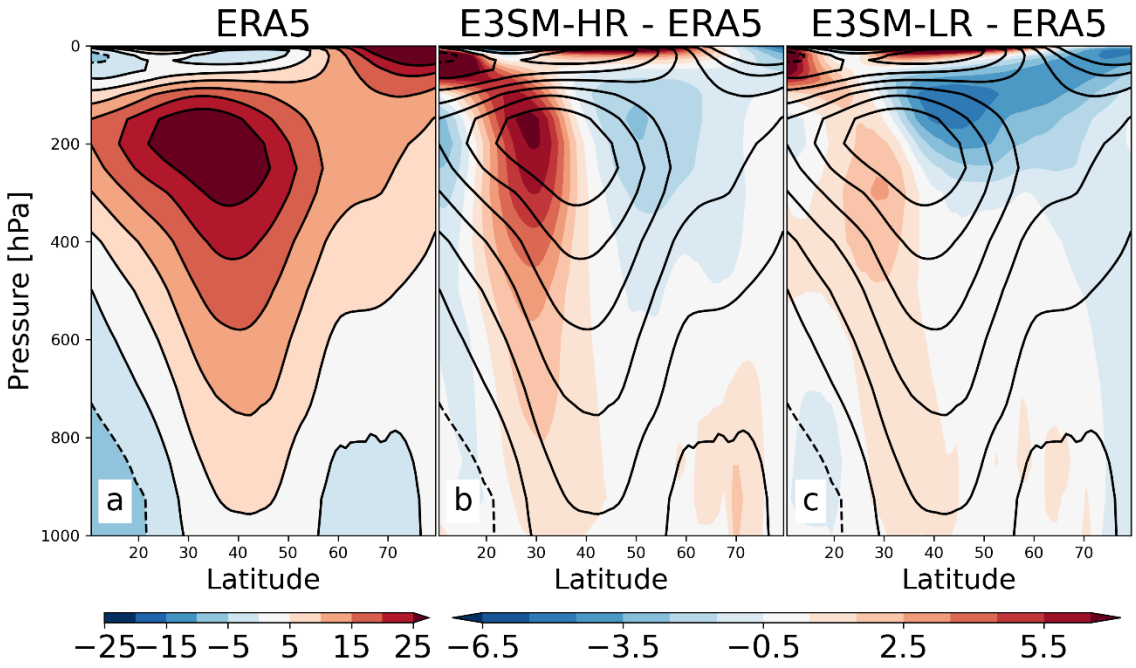

Figure 5. Zonal winds averaged between over the Northern Pacific (180-110W) for NDJFM for ERA5 (a), and the differences between E3SM-HR and ERA5 (b) as well as E3SM-LR and ERA5 (c). The black contours in each panel are equal to the climatological ERA5 values. Units are given in m/s.

3.2 Heat Waves

We begin by examining the 95th percentile daily maximum temperature for May through September (MJJAS) in ERA5, as well as E3SM-HR and E3SM-LR along the US West Coast (Figure 6). The 95th percentile daily maximum temperature distribution agrees better with ERA5 in E3SM-HR than in E3SM-LR. Figure 6 shows the errors measured by the RMSE decrease at high resolution and the IoA shows better agreement with ERA5 for high resolution. The 95th percentile daily maximum temperature tends to be too cold for E3SM-LR relative to ERA5.

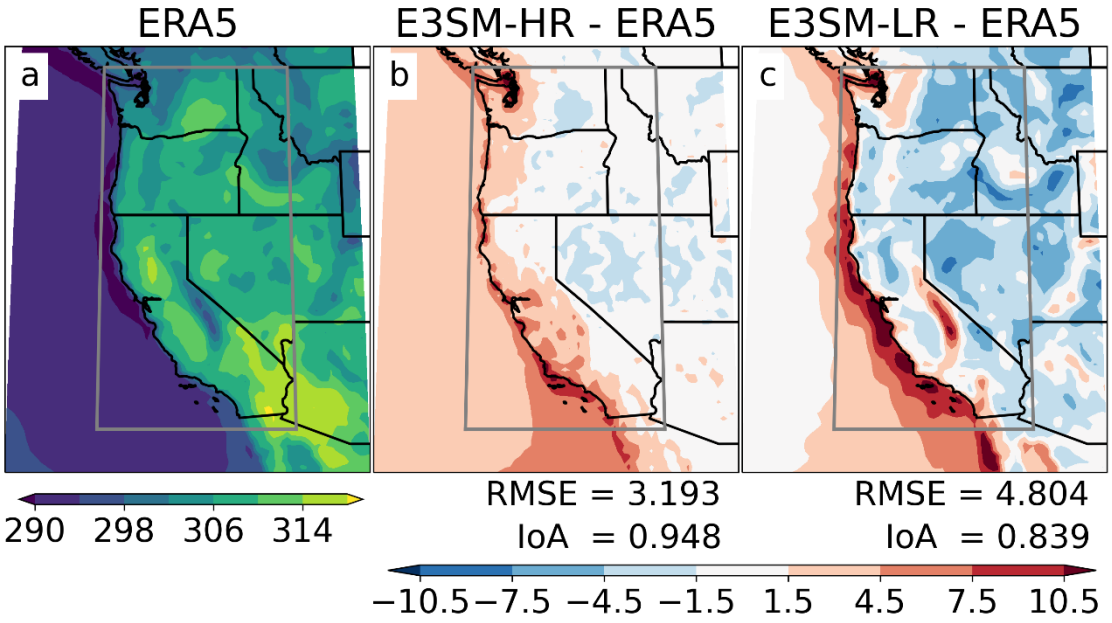

Figure 6. MJJAS 95th percentile daily maximum temperature for ERA5 (a). Differences between E3SM-HR and ERA5 (b) and between E3SM-LR and ERA5 (c). Units are K.

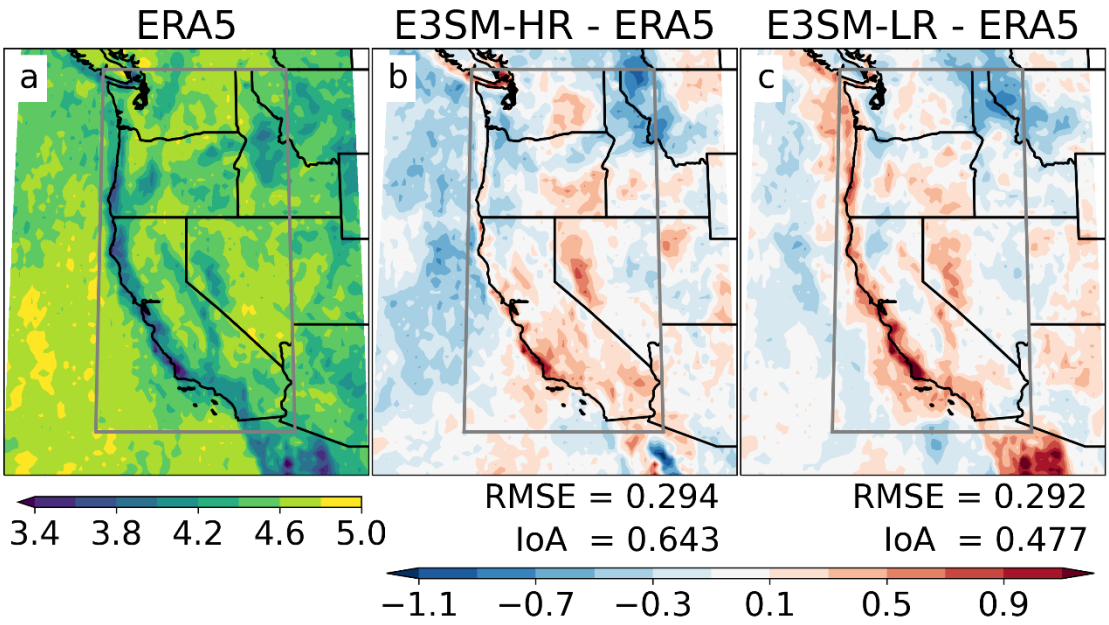

Figure 7. Heat wave frequency in ERA5, and differences between E3SM-HR and ERA5, as well as E3SM-LR and ERA5. Units are number of days.

Frequency, intensity, and duration are all important measures of HWs, and we quantify the biases for all three for E3SM here. HW frequency, intensity, and duration are defined as the number of HW days, the average daily maximum temperature during HW days, and the average number of days each HW lasts, respectively. Figure 7 shows the frequency of heat waves for both E3SM-HR and E3SM-LR compared to ERA5. The magnitudes of biases in HW frequency for E3SM-HR and E3SM-LR are quite similar along the US West Coast. The RMSE relative to ERA5 is nearly identical for the two simulations as well. The IoA, however, shows improvement for E3SM-HR over E3SM-LR, suggesting there may be marginal improvement in HW frequency when increasing horizontal grid spacing.

Figures 8 and 9 show clear improvements for HW intensity and duration, respectively, for E3SM-HR when compared to E3SM-LR. Errors are smaller (lower RMSE) and agreement is greater (higher IoA) for both intensity and duration in E3SM-HR than in E3SM-LR. Like the 95th percentile daily max temperature, which was too cold in E3SM-LR relative to ERA5, the departure of temperature during a HW event is also too cold. The biases in HW intensity are much smaller for E3SM-HR, rarely beyond 3 K.

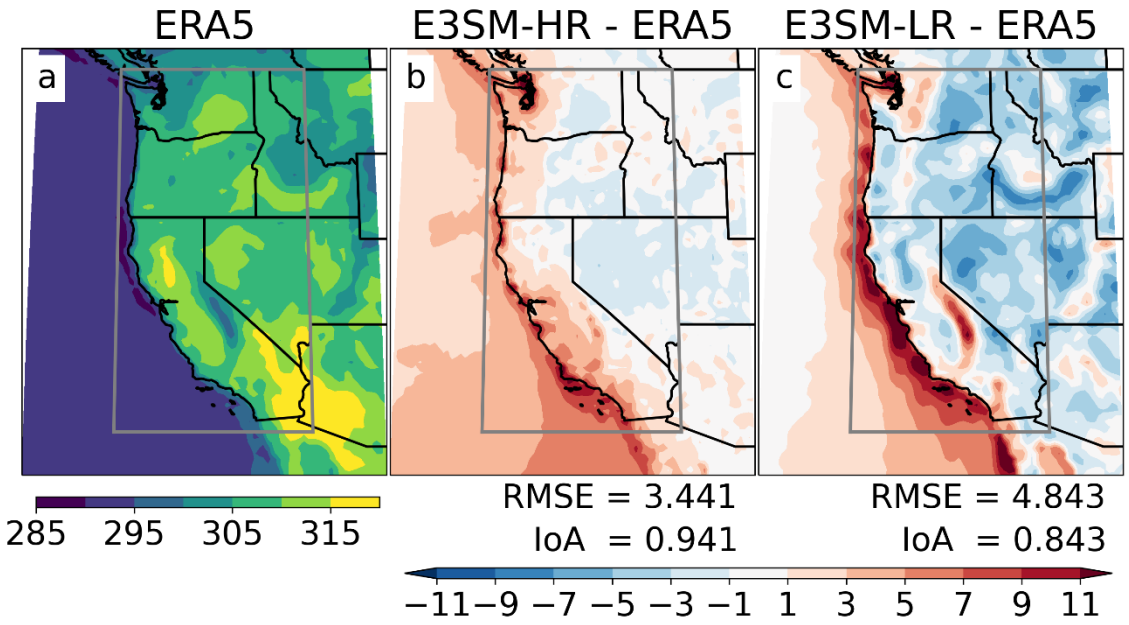

Figure 8. As in Figure 7, only for HW intensity. Units are K.

Both E3SM-LR and E3SM-HR tend to overestimate the duration of HW events, but those biases are improved upon with higher resolution. The large bias in HW duration over the Southwest in E3SM-LR is significantly reduced in E3SM-HR. The E3SM-LR biases in the Northwest are nearly absent in E3SM-HR. Overall, increased horizontal resolution improves the representation of both HW intensity and duration, without any degradation in the representation of HW frequency.

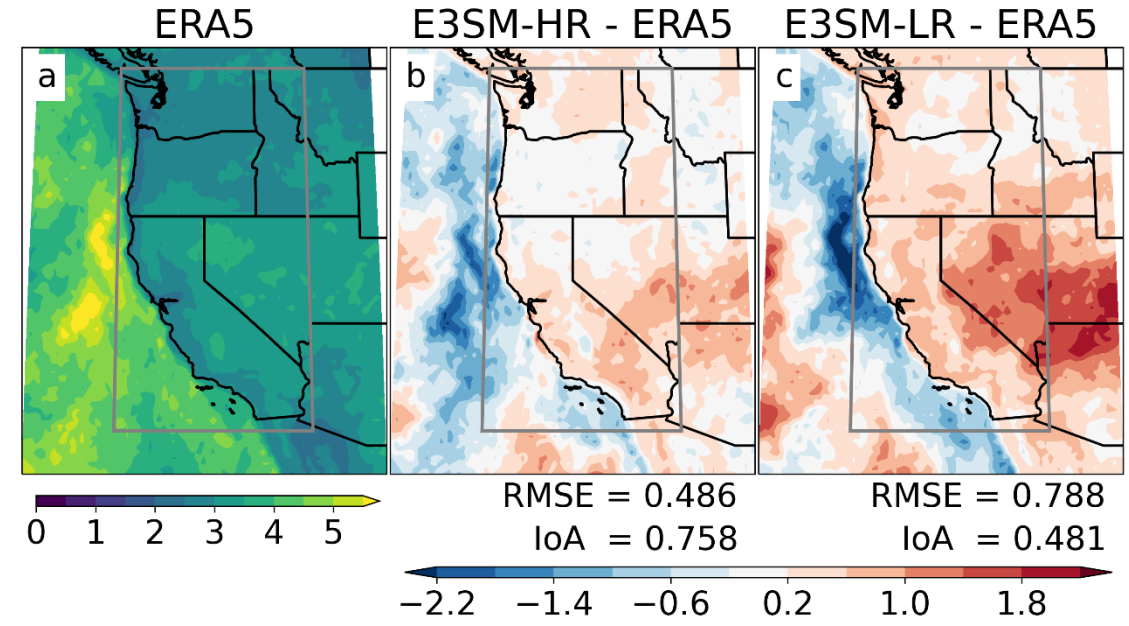

Figure 9. As in Figure 7, only for HW duration. Units are number of days.

Summarizing the evaluation of ARs and HWs in the E3SMv1 HR and LR simulations, increasing the model grid spacing from ~100 km to ~25 km generally results in improvements in representing the two types of extreme weather events in the western US. Most notably, increasing model resolution improves the simulation of extreme precipitation (Figure 3) and strong winds (Figure 2) associated with ARs and heat wave intensity (Figure 8) and duration (Figure 9). For ARs, the improvements are likely related to the ability of the model to better represent topographic effects on precipitation and lower tropospheric circulation at higher resolution, which captures the complex terrain of the western US more realistically. At higher resolution, the ability to simulate sharper gradients of moisture and winds associated with the AR frontal systems may also contribute to improving modeling of AR extreme precipitation and strong winds. For HWs, improvements in modeling HW intensity at higher resolution reflect the cold bias of the 95th percentile daily maximum temperature in the LR simulation (Figure 6), which may be related to improved representation of the complex terrain and associated bias reductions in cloud cover, low level moisture, precipitation, shortwave and longwave radiation, and land-atmosphere interactions, which may also improve simulation of HW duration.

Although increasing model resolution generally improves the simulation of ARs and HWs, particularly on intensity related metrics, AR and HW frequencies are not very sensitive to model resolution. Noticeably, a slight degradation is even found in AR frequency, location, and geometry (length and width) at higher resolution. The frequency and spatial distribution of extreme weather events are arguably more strongly influenced by large-scale circulation features such as the North Pacific jet stream for ARs (Hagos et al. 2016; Gao et al. 2015) and large-scale meteorological patterns such as related to atmospheric blocking and modes of climate variability for HWs (Grotjahn et al. 2016). As large-scale circulations are more dominantly influenced by processes such as tropical convection and atmosphere-ocean interactions that determine the spatial distribution of diabatic heating, simply increasing model resolution without significant efforts to calibrate model parameters and improve physics parameterizations does not guarantee improvements in modeling large-scale circulation features. Hence to improve modeling of frequency, intensity, and other aspects of extreme weather events such as ARs and HWs, more efforts are needed in Earth system modeling to address parametric and structural uncertainties of physics parameterizations and their sensitivity and scale-awareness across model resolutions.

4.0 References

Caldwell, P. M., Mametjanov, A., Tang, Q., Van Roekel, L. P., Golaz, J. C., Lin, W., Bader, D. C., Keen, N. D., Feng, Y., Jacob, R., Maltrud, M. E., Roberts, A. F., Taylor, M. A., Veneziani, M., Wang, H., Wolfe, J. D., Balaguru, K., Cameron-Smith, P., Dong, L., . . . Zhou, T. (2019). The DOE E3SM Coupled Model Version 1: Description and Results at High Resolution. In *Journal of Advances in Modeling Earth Systems* (Vol. 11, pp. 4095-4146).

Dennis, J. M., Edwards, J., Evans, K. J., Guba, O., Lauritzen, P. H., Mirin, A. A., St-Cyr, A., Taylor, M. A., & Worley, P. H. (2012). CAM-SE: A scalable spectral element dynamical core for the Community Atmosphere Model. In *International Journal of High Performance Computing Applications* (Vol. 26, pp. 74-89).

Gent, P. R., & Mcwilliams, J. C. (1990). Isopycnal Mixing in Ocean Circulation Models. In *Journal of Physical Oceanography* (Vol. 20, pp. 150-155).

Gettelman, A., & Morrison, H. (2015). Advanced two-moment bulk microphysics for global models. Part I: Off-line tests and comparison with other schemes. In *Journal of Climate* (Vol. 28, pp. 1268-1287).

Gettelman, A., Morrison, H., Santos, S., Bogenschutz, P., & Caldwell, P. M. (2015). Advanced two-moment bulk microphysics for global models. Part II: Global model solutions and aerosol-cloud interactions. In *Journal of Climate* (Vol. 28, pp. 1288-1307).

Golaz, J.-C., Larson, V. E., & Cotton, W. R. (2002). A PDF-Based Model for Boundary Layer Clouds. Part I: Method and Model Description. In *Journal Of The Atmospheric Sciences* (Vol. 59, pp. 3540-3551).

Hagos, S. M., Leung, L. R., Yoon, J. H., Lu, J., & Gao, Y. (2016). A projection of changes in landfalling atmospheric river frequency and extreme precipitation over western North America from the Large Ensemble CESM simulations. *Geophysical Research Letters*, *43*(3), 1357-1363. https://doi.org/10.1002/2015gl067392

Hersbach, H., Bell, B., Berrisford, P., Hirahara, S., Horányi, A., Muñoz-Sabater, J., Nicolas, J., Peubey, C., Radu, R., Schepers, D., Simmons, A., Soci, C., Abdalla, S., Abellan, X., Balsamo, G., Bechtold, P., Biavati, G., Bidlot, J., Bonavita, M., . . . Thépaut, J. N. (2020). The ERA5 global reanalysis. In *Quarterly Journal of the Royal Meteorological Society* (Vol. 146, pp. 1999-2049).

Huang, C., Barnett, A. G., Wang, X., Vaneckova, P., FitzGerald, G., & Tong, S. (2011). Projecting future heat-related mortality under climate change scenarios: a systematic review. *Environ Health Perspect*, *119*(12), 1681-1690. https://doi.org/10.1289/ehp.1103456

Huffman, G. J., Bolvin, D. T., Nelkin, E. J., & Tan, J. (2017). Integrated Multi-satellitE Retrievals for GPM (IMERG) Technical Documentation. *IMERG Tech Document*, *158*(March), 54.

Iacono, M. J., Delamere, J. S., Mlawer, E. J., Shephard, M. W., Clough, S. A., & Collins, W. D. (2008). Radiative forcing by long-lived greenhouse gases: Calculations with the AER radiative transfer models. In *Journal of Geophysical Research* (Vol. 113, pp. D13103).

Inda-Díaz, H. A., O'Brien, T. A., Zhou, Y., & Collins, W. D. (2021). Constraining and Characterizing the Size of Atmospheric Rivers: A Perspective Independent From the Detection Algorithm. *Journal of Geophysical Research: Atmospheres*, *126*(16). https://doi.org/10.1029/2020jd033746

Larson, V. E. (2017). CLUBB-SILHS: A parameterization of subgrid variability in the atmosphere. In *arXiv*.

Larson, V. E., & Golaz, J.-C. (2005). Using Probability Density Functions to Derive Consistent Closure Relationships among Higher-Order Moments. In *Monthly Weather Review* (Vol. 133, pp. 1023-1042).

Leung, L. R., Boos, W. R., Catto, J. L., Demott, C. A., Martin, G. M., Neelin, J. D., O'Brien, T. A., Xie, S., Feng, Z., Klingaman, N. P., Kuo, Y. H., Lee, R. W., Martinez-Villalobos, C., Vishnu, S., Priestley, M. D. K., Tao, C., & Zhou, Y. (2022). Exploratory Precipitation Metrics: Spatiotemporal Characteristics, Process-Oriented, and Phenomena-Based. In *Journal of Climate* (Vol. 35, pp. 3659-3686).

Li, H., Wigmosta, M. S., Wu, H., Huang, M., Ke, Y., Coleman, A. M., & Leung, L. R. (2013). A physically based runoff routing model for land surface and earth system models. In *Journal of Hydrometeorology* (Vol. 14, pp. 808-828).

Li, H. Y., Leung, L. R., Getirana, A., Huang, M., Wu, H., Xu, Y., Guo, J., & Voisin, N. (2015). Evaluating global streamflow simulations by a physically based routing model coupled with the community land model. In *Journal of Hydrometeorology* (Vol. 16, pp. 948-971).

Liu, X., Chang, P., Fu, D., Saravanan, R., Wang, H., Rosenbloom, N., Zhang, S., & Wu, L. (2022). Improved Simulations of Atmospheric River Climatology and Variability in High-Resolution CESM. In *Journal of Advances in Modeling Earth Systems* (Vol. 14, pp. 1-18).

Liu, X., Ma, P. L., Wang, H., Tilmes, S., Singh, B., Easter, R. C., Ghan, S. J., & Rasch, P. J. (2016). Description and evaluation of a new four-mode version of the Modal Aerosol Module (MAM4) within version 5.3 of the Community Atmosphere Model. In *Geoscientific Model Development* (Vol. 9, pp. 505-522).

Lu, J., Chen, G., Leung, L. R., Burrows, D. A., Yang, Q., Sakaguchi, K., & Hagos, S. (2015). Toward the dynamical convergence on the jet stream in aquaplanet AGCMs. In *Journal of Climate* (Vol. 28, pp. 6763-6782).

Lu, J., Xue, D., Gao, Y., Chen, G., Leung, L. R., & Staten, P. (2018). Enhanced hydrological extremes in the western United States under global warming through the lens of water vapor wave activity. *npj Climate and Atmospheric Science*, *1*(1). https://doi.org/10.1038/s41612-018-0017-9

Mlawer, E. J., Taubman, S. J., Brown, P. D., Iacono, M. J., & Clough, S. A. (1997). Radiative transfer for inhomogeneous atmospheres: RRTM, a validated correlated-k model for the longwave. In *Journal of Geophysical Research* (Vol. 102, pp. 16663-16682).

Neale, R. B., Richter, J. H., & Jochum, M. (2008). The impact of convection on ENSO: From a delayed oscillator to a series of events. In *Journal of Climate* (Vol. 21, pp. 5904-5924).

Oleson, K. W., Lawrence, D. M., Bonan, G. B., Drewniak, B., Huang, M., Koven, C. D., Levis, S., Li, F., Riley, W. J., Subin, Z. M., Swenson, S. C., Thornton, P. E., Bozbiyik, A., Fisher, R., Heald, C. L., Kluzek, E., Lamarque, J.-F., Lawrence, P. J., Leung, L. R., . . . Yang, Z.-L. (2013). Technical description of version 4.5 of the Community Land Model (CLM). In *NCAR/TN-478+STR NCAR Technical Note* (pp. 266).

Petersen, M. R., Asay-Davis, X. S., Berres, A. S., Chen, Q., Feige, N., Hoffman, M. J., Jacobsen, D. W., Jones, P. W., Maltrud, M. E., Price, S. F., Ringler, T. D., Streletz, G. J., Turner, A. K., Van Roekel, L. P., Veneziani, M., Wolfe, J. D., Wolfram, P. J., & Woodring, J. L. (2019). An Evaluation of the Ocean and Sea Ice Climate of E3SM Using MPAS and Interannual CORE-II Forcing. In *Journal of Advances in Modeling Earth Systems* (Vol. 11, pp. 1438-1458).

Rasch, P. J., Xie, S., Ma, P. L., Lin, W., Wang, H., Tang, Q., Burrows, S. M., Caldwell, P., Zhang, K., Easter, R. C., Cameron-Smith, P., Singh, B., Wan, H., Golaz, J. C., Harrop, B. E., Roesler, E., Bacmeister, J., Larson, V. E., Evans, K. J., . . . Yang, Y. (2019). An Overview of the Atmospheric Component of the Energy Exascale Earth System Model. In *Journal of Advances in Modeling Earth Systems* (Vol. 11, pp. 2377-2411).

Rhoades, A. M., Risser, M. D., Stone, D. A., Wehner, M. F., & Jones, A. D. (2021). Implications of warming on western United States landfalling atmospheric rivers and their flood damages. In *Weather and Climate Extremes* (Vol. 32).

Richter, J. H., & Rasch, P. J. (2008). Effects of Convective Momentum Transport on the Atmospheric Circulation in the Community Atmosphere Model, Version 3. In *Journal of Climate* (Vol. 21, pp. 1487-1499).

Ringler, T., Petersen, M., Higdon, R. L., Jacobsen, D., Jones, P. W., & Maltrud, M. (2013). A multi-resolution approach to global ocean modeling. In *Ocean Modelling* (Vol. 69, pp. 211-232): Elsevier Ltd.

Seneviratne, S. I., X. Zhang, M. Adnan, W. Badi, C. Dereczynski, A. Di Luca, S. Ghosh, I. Iskandar, J. Kossin, S. Lewis, F. Otto, I. Pinto, M. Satoh, S.M. Vicente-Serrano, M. Wehner, and B. Zhou. (2021). *Weather and Climate Extreme Events in a Changing Climate* (Climate Change 2021: The Physical Science Basis. Contribution of Working Group I to the Sixth Assessment Report of the Intergovernmental Panel on Climate Change, Issue. C. U. Press.

Shields, C. A., Rutz, J. J., Leung, L.-Y., Ralph, F. M., Wehner, M., Kawzenuk, B., Lora, J. M., McClenny, E., Osborne, T., Payne, A. E., Ullrich, P., Gershunov, A., Goldenson, N., Guan, B., Qian, Y., Ramos, A. M., Sarangi, C., Sellars, S., Gorodetskaya, I., . . . Nguyen, P. (2018). Atmospheric River Tracking Method Intercomparison Project (ARTMIP): project goals and experimental design. *Geoscientific Model Development*, *11*(6), 2455-2474. https://doi.org/10.5194/gmd-11-2455-2018

Ullrich, P. A., & Zarzycki, C. M. (2017). TempestExtremes: A framework for scale-insensitive pointwise feature tracking on unstructured grids. In *Geoscientific Model Development* (Vol. 10, pp. 1069-1090).

Ullrich, P. A., Zarzycki, C. M., McClenny, E. E., Pinheiro, M. C., Stansfield, A. M., & Reed, K. A. (2021). TempestExtremes v2.1: a community framework for feature detection, tracking, and analysis in large datasets. *Geoscientific Model Development*, *14*(8), 5023-5048. https://doi.org/10.5194/gmd-14-5023-2021

Wang, H., Easter, R. C., Zhang, R., Ma, P. L., Singh, B., Zhang, K., Ganguly, D., Rasch, P. J., Burrows, S. M., Ghan, S. J., Lou, S., Qian, Y., Yang, Y., Feng, Y., Flanner, M., Leung, L. R., Liu, X., Shrivastava, M., Sun, J., . . . Yoon, J. H. (2020). Aerosols in the E3SM Version 1: New Developments and Their Impacts on Radiative Forcing. *Journal of Advances in Modeling Earth Systems*, *12*(1). https://doi.org/10.1029/2019ms001851

Ye, X., Wolff, R., Yu, W., Vaneckova, P., Pan, X., & Tong, S. (2012). Ambient temperature and morbidity: a review of epidemiological evidence. *Environ Health Perspect*, *120*(1), 19-28. https://doi.org/10.1289/ehp.1003198

Zhang, G. J., & McFarlane, N. A. (1995). Sensitivity of climate simulations to the parameterization of cumulus convection in the Canadian climate centre general circulation model. In *Atmosphere-Ocean* (Vol. 33, pp. 407-446).

Zhu, Y., & Newell, R. E. (1998). A proposed algorithm for moisture fluxes from atmospheric rivers. In *Monthly Weather Review* (Vol. 126, pp. 725-735).

U.S. DEPARTMENT OF
ENERGY

Office of Science